THE JOURNAL OF PHYSICAL CHEMISTRY A

Article

Bifunctional Hydrogen Bonding of Imidazole with Water Explored by Rotational Spectroscopy and DFT Calculations

Eva Gougoula, Daniel J Cole, and Nicholas R. Walker

J. Phys. Chem. A, **Just Accepted Manuscript** • DOI: 10.1021/acs.jpca.0c00544 • Publication Date (Web): 06 Mar 2020

is published by the American Chemical Society. 1155 Sixteenth Street N.W., Washington, DC 20036

Journal of Physical Chemistry A

Bifunctional Hydrogen Bonding of Imidazole with Water Explored by Rotational Spectroscopy and DFT Calculations

Eva Gougoula, Daniel J. Cole and Nicholas R. Walker

Chemistry- School of Natural and Environmental Sciences, Newcastle University, Bedson Building, Newcastle upon Tyne, NE1 7RU, UK

Corresponding author: Nick.Walker@newcastle.ac.uk

ABSTRACT

Laser vaporisation of imidazole in the presence of an argon buffer gas has allowed the generation and isolation of two isomers of an imidazole monohydrate complex, denoted herein as imid···H_2O and H_2O···imid, within a gas sample undergoing supersonic expansion. Imidazole and water are respectively proton-accepting and proton-donating in imid···H_2O but these roles are reversed in the H_2O···imid complex. Both isomers have been characterised by chirped-pulse Fourier transform microwave spectroscopy between 7.0 and 18 GHz. The ground-state rotational spectra of four isotopologues of imid···H_2O and three isotopologues of H_2O···imid have been measured. All spectra have been assigned and fitted to determine rotational (A_0, B_0, C_0), centrifugal distortion (D_J, D_{JK}) and nuclear quadrupole coupling constants, (χ_{aa}(N1), [χ_{bb}(N1) − χ_{cc}(N1)], χ_{aa}(N3) and [χ_{bb}(N3) − χ_{cc}(N3)]). Structural parameters (r_0 and r_s) have been accurately determined from measured rotational constants for each isomer. The imid···H_2O complex contains a non-linear hydrogen bond (∠(O–H_b···N3=172.1(26)° in the experimentally-determined, r_0 geometry) between the pyridinic nitrogen of imidazole and a hydrogen atom of H_2O. The DFT calculations find that the H_2O···imid complex also contains a non-linear hydrogen bond between the oxygen atom of water and the hydrogen attached to the pyrrolic nitrogen of imidazole (∠(O···H1–N1)=174.7°). Two states observed in the spectrum of H_2O···imid, assigned as 0^- and 0^+ states, confirm that large amplitude motions occur on the timescale of the molecular rotation. Density functional theory has been performed to characterise these large amplitude motions.

1. INTRODUCTION

Imidazole[1] is a five-membered aromatic ring that is an important building block of biomolecules such as the nucleobase adenine and the amino-acid histidine. It can interact with haemoglobin[2] through either its pyrrolic or its pyridinic nitrogen as either proton donor or proton acceptor respectively. Anti-cancer agents such as *cis*-Pt drugs[3] bind to guanine or adenine components of DNA while stabilised by secondary interactions with the pyridinic nitrogen of the imidazole subunit. The structure of solid imidazole has been determined through neutron[4] and X-ray[5] diffraction experiments. In the solid state, under ambient conditions, individual imidazole molecules[5] form into "daisy chains" with linkages at both the pyrrolic and pyridinic nitrogen atoms of individual molecules. Microwave spectroscopy allows for precise measurements of molecular structure in complexes formed between imidazole and other small molecules in the gas phase[6,7]. Such experiments allow the binding properties of molecules that contain an imidazole ring to be rationalised in the absence of a solvent or matrix. The imidazole dimer characterised by Mullaney *et al.*[7] was shown to contain an intermolecular hydrogen bond between the pyrrolic nitrogen of one monomer and the pyridinic nitrogen of another.

It is possible to explore the step-wise hydration of aromatic molecules through studies of gas phase complexes formed by these molecules with water[8–15]. The two nitrogen atoms of imidazole are far enough apart that an individual water molecule may interact with either the pyrrolic or the pyridinic site but not both simultaneously. The geometries of monohydrate complexes have previously been characterised through microwave spectroscopy for *N*-heteroaromatics that include indole[13] (C_8H_7N), pyrrole[12] (C_4H_5N), isoxazole[15] (C_3H_3NO), pyridine[9] (C_5H_5N), pyrimidine[10] ($C_4H_4N_2$) and pyridazine[11] ($C_4H_4N_2$). Chemical environment determines the binding site selected by the water molecule. A hydrogen bond forms between the pyrrolic nitrogen of the ring and the oxygen atom of the water in each of $H_2O\cdots$pyrrole[12]

and H_2O···indole[13]. Water acts as proton donor, and the pyridinic nitrogen acts as proton acceptor, in the monohydrates of pyridine[9], isoxazole[15], pyrimidine[10] and pyridazine[11]. IR spectroscopy of complexes isolated in helium nanodroplet matrices[16] previously identified two isomers of a complex formed between imidazole and water. In the first isomer, imid···H_2O, water acts as proton donor and the pyridinic nitrogen atom of imidazole acts as proton acceptor. In the second isomer, H_2O···imid, the pyrrolic site of the imidazole ring acts as proton donor while H_2O acts as proton acceptor.

A subsequent experiment[17] employed IR spectroscopy to probe complexes formed within a free jet expansion and observed only the isomer in which water acts as the proton donor. More recent IR spectroscopic experiments[18,19] probed benzimidazole ($C_7H_6N_2$) molecules isolated in the gas phase and identified both an isomer where H_2O is attached to the pyrrolic site and another where it is bound to the pyridinic site of the imidazole sub-unit. In the present work, the two isomers of imidazole monohydrate identified previously by matrix isolation experiments, imid···H_2O and H_2O···imid, have both been characterised while isolated in the gas phase. Broadband rotational spectra of both isomers are reported and analysed to accurately determine geometrical parameters which include the length of the hydrogen bond and the orientation of the water molecule for each isomer. Evidence for large amplitude motions in the spectrum of H_2O···imid is described. The labels used herein to distinguish the two isomers respect the standard convention that the Lewis base (hydrogen bond acceptor) precedes the Lewis acid (hydrogen bond donor) when labelling a complex bound by a single hydrogen bond.

2. EXPERIMENTAL METHODS

Both the laser vaporisation source and the CP-FTMW spectrometer used by the present experiments has been described in detail elsewhere[20–22]. The focussed pulse of a Nd:YAG laser (Photonics Solutions, Minilite II, 1064 nm, 43 mJ pulse^{-1}) is used to vaporise a solid target of imidazole to generate the gaseous sample required by the spectroscopic experiments. When performing experiments on the parent isotopologues of imid···H_2O and H_2O···imid, a solid matrix of silver iodide (Fisher Scientific, 99%, ACROS Organics^{TM}) was used while experiments performed on D_2O/HDO-containing isotopologues employed a copper powder (Sigma-Aldrich, <75 μm, 99%) matrix. In each experiment, the imidazole sample was mixed with the matrix in a 1:1 ratio before being pressed into a solid target rod of 13 mm in diameter. The focussed laser pulse irradiates the surface of the prepared rod at a short distance from the orifice of a pulse valve (Parker, Series 9) which introduces an argon (BOC, 99.998%) buffer gas into a vacuum chamber. Vaporised sample becomes entrained within the argon flow which subsequently undergoes supersonic expansion.

Empirical factors led to the selection of different matrices for the various experiments. Transitions of diatomic AgI were useful for instrument calibration during initial survey scans that revealed the spectrum of the parent isotopologue. In order to reduce spectral congestion (by eliminating AgI signals from the spectrum), subsequent experiments were performed while using copper powder matrices. Water was incidentally present in either the argon gas sample or the pressed solid sample as a contaminant so no deliberate actions were necessary to introduce it. Subsequent to experiments on parent isotopologues, experiments were performed using isotopically-enriched samples of HDO and $H_2{}^{18}O$ to allow determination of the position and orientation of the water molecule with respect to the imidazole ring. Approximately 0.1 mL of D_2O (Sigma-Aldrich, 99.9% D atom) was placed into a bespoke reservoir that attaches onto the faceplate of the pulse valve and directly seeded into the flow of the expanding jet of argon. Isotopic substitution with residual contaminant H_2O allowed the spontaneous formation

of HDO from the D_2O and H_2O present within the gas sample. The spectra of isotopologues containing $H_2{}^{18}O$ were recorded during a separate experiment where $H_2{}^{18}O$ (Sigma-Aldrich, 97% atom ^{18}O) was introduced into the spectrometer by the same method.

The rotational spectra of imid···H_2O and H_2O···imid were recorded between 7.0 and 18.5 GHz. The CP-FTMW spectrometer mixes a microwave pulse that linearly sweeps from 12.0 to 0.5 GHz over a duration of 1 μs against the 19 GHz reference signal of a Phase-locked Dielectric Resonant Oscillator (PDRO). Chirped pulses are generated from a 20 GS/s arbitrary waveform generator (AWG) (Tektronix AWG 7102). A low pass filter selects the 7.0-18.5 GHz sideband which is amplified by a 300 W Traveling-Wave Tube Amplifier (TWT) prior to its introduction from a horn antenna into the vacuum chamber perpendicular to the direction of the expanding gas jet. Subsequent to the molecular polarisation, the free induction decay (which has duration of 20 μs) of the molecular emission is detected by a second horn antenna and digitally recorded by a 100 GS/s oscilloscope (Tektronix DPO72304XS). Successive free induction decays are co-added in the time domain. The polarisation pulse and free induction decay are each sufficiently short that eight distinct measurements of the broadband microwave spectrum are routinely performed following each gas introduction pulse while taking advantage of the "fast frame" mode of the oscilloscope. A high resolution window function was used by the Fourier transform employed herein such that linewidths of transitions in the frequency domain spectrum are approximately 100 kHz for a well-isolated line at full-width half-maximum. This linewidth correlates with an estimated accuracy of 10 kHz in the measurement of line centre frequencies. Phase coherence in the time domain and accuracy in transition frequencies was provided by an Rb-clock (SRS FS725) to which the AWG, the PDRO and the oscilloscope were phase-locked.

3. DENSITY FUNCTIONAL THEORY CALCULATIONS

Optimisations of the geometries of imid···H_2O and H_2O···imid were performed using the Gaussian09 package[23]. The harmonic hybrid functional[24–26] of Becke, Lee, Yang, Parr, B3LYP, in conjunction with Grimme's dispersion correction effects[27] and damping function[28], D3BJ, was initially used alongside Dunning's[29,30] augmented triple zeta aug-cc-pVTZ basis set. Geometry optimisations were subsequently performed with the long range corrected hybrid functional[31], ωB97X-D, of Chai and Gordon and Dunning's augmented quadrupole zeta basis set with tight convergence criteria. Grimme's D2 dispersion correction[27] was included in the functional. Calculated values of rotational constants and dipole moment components are presented in Table 1. The complete set of DFT-calculated atomic coordinates is presented in Table S1 of the supplementary information. For H_2O···imid, one-dimensional potential energy surfaces (PES) were scanned to describe large amplitude motions in each of two internal coordinates. These respectively probe the torsional and wagging motions of H_2O with respect to the imidazole ring and are presented in Section 4. Calculated rotational constants (A_e, B_e and C_e), dipole moment components ($|\mu_a|$, $|\mu_b|$ and $|\mu_c|$) and relative energies of the two complexes are summarised in Table 1. Due to its strong performance across a wide range of benchmark tests[32], structural parameters calculated at the ωB97X-D/aug-cc-pVQZ level will be used in the comparisons to follow.

4. RESULTS

Spectral Assignment and Analysis. DFT calculations were initially guided by previous studies[9,12] of pyridine···H_2O and H_2O···pyrrole. Detailed conformational searches were not necessary because of inferences drawn from these previous works and the simple, well-known

geometries of each monomer sub-unit. The minimum energy configuration of each of imid···H_2O and H_2O···imid is a near-prolate symmetric rotor (Figure 1). All heavy atoms lie in the plane defined by the imidazole ring and the electric dipole moment of the complex is nearly colinear with the *a*-inertial axis in each isomer. The hydrogen atoms of the water sub-unit, except for the bound hydrogen in imid···H_2O, lie outside of the plane defined by the heavy atoms in the DFT-calculated geometries. The broadband microwave spectrum recorded under the described experimental conditions is displayed in Figure 2. The most intense transitions are those assigned to the imidazole monomer[1]. Rotational transitions of $(imid)_2$, imid···Ar, AgI and $(H_2O)_2$ were readily assigned with reference to previous studies[6,7,33–35]. Products of fragmentation of imidazole and gas phase chemical reactions are also present in the spectra. Molecular species identified[36–44] include HC_3N, HC_5N, HC_7N, HC_9N, CH_3CN, ICN, IC_3N, C_4H_3N (methylcyanoacetylene), C_4H_3N (cyanoallene) and C_3H_2N (vinyl cyanide).

Additional to transitions of the aforementioned species, others that are consistent with expectations for the spectra of H_2O···imid and imid···H_2O are apparent. Hyperfine splittings confirm the presence of two distinct nitrogen nuclei in the molecular carriers of these spectra. Assignment and fitting of spectroscopic transitions was performed using Watson's *S* reduced Hamiltonian[45] in the I^r representation as implemented in Western's PGOPHER[46].

$$H = H_{\mathrm{R}} - \frac{1}{6}\mathbf{Q}(\mathrm{N1}):\nabla\mathbf{E}(\mathrm{N1}) - \frac{1}{6}\mathbf{Q}(\mathrm{N3}):\nabla\mathbf{E}(\mathrm{N3}), \qquad (1)$$

where H_{R} is the energy operator for a semi-rigid asymmetric rotor and the remaining terms represent interactions between the nuclear electric quadrupole moment and the electric field gradient at each nitrogen atom. The formulation of H_{R} included A_0, B_0 and C_0 rotational constants and D_J and D_{JK} centrifugal distortion constants when fitting the parent isotopologue of each of imid···H_2O and H_2O···imid. The nuclear quadrupole moment dyadic is represented

by **Q** and the dyadic of the electric field gradient is $\nabla\mathbf{E}$. Components of the nuclear quadrupole coupling tensor of each quadrupolar nitrogen nucleus are denoted by χ_{aa} and $(\chi_{bb} - \chi_{cc})$ with nitrogen atoms numbered according to the usual convention for heteroaromatic molecules with N1 and N3 denoting the pyrrolic and pyridinic nitrogen atoms respectively. Matrix elements were constructed in the coupled asymmetric rotor basis, $\boldsymbol{J} + \boldsymbol{I}_{\mathrm{N1}} = \boldsymbol{F}_1$, $\boldsymbol{F} + \boldsymbol{I}_{\mathrm{N3}} = \boldsymbol{F}_2$, and diagonalised in blocks of the quantum number, F. When fitting the data for imid···$H_2{}^{18}O$, imid···H_bOD_{nb} and the 0^+ state of HDO…imid (Tables S2 and S3), it was found necessary to include the additional centrifugal distortion term, d_1, to obtain a satisfactory fit. The assignment of the χ_{aa} and $(\chi_{bb} - \chi_{cc})$ values to the correct nitrogen nucleus was achieved on basis of DFT calculations of the same quantities as shown in Table S4. The projection of nuclear quadrupole coupling tensors onto inertial axes is sensitive to molecular geometry so the good agreement between the experimental and calculated values confirms the basic geometries of these complexes to be as shown in Figure 1. Values of χ_{xx} , χ_{yy} and χ_{zz}, which are projections of each nuclear quadrupole coupling tensor onto principal axes located on each individual nucleus are presented in Table S5.

Transitions were initially tentatively assigned to the imid···H_2O complex based on similarities between the fitted rotational constants and those calculated using DFT for this isomer. The assignment of *a*-type transitions having $\Delta J = 1$ and $\Delta K = 0$ allows determination of the spectroscopic parameters summarized in the first column of Table 2. Spectra of different tunnelling states were reported for pyridine···H_2O, isoxazole···H_2O and pyrazine···H_2O complexes[8,9,15]. The spectra of imid···H_2O do not contain such splittings and in this respect, the results are more consistent with those reported for pyrimidine···H_2O and 2-fluoropyridine···H_2O where only a single state was observed for each complex[10,14]. The observation of *a*- and *b*-type (but not *c*-type) transitions for spectra of all isotopologues of imid···H_2O is consistent with a

planar geometry for this complex. Further examination of the data revealed additional transitions that can be independently assigned to two different states, denoted as 0^- and 0^+, of a spectrum assigned to $H_2O\cdots$imid. The fitted rotational and centrifugal distortion constants of each state of this spectrum are very similar and shown in the 2nd and 3rd columns of Table 2. Transitions assigned to the 0^- state are more intense, by a factor of three, than those assigned to the 0^+ state. The spectra reported for each of $H_2O\cdots$indole and $H_2O\cdots$pyrrole also contain 0^- and 0^+ states (with statistical intensity weights of 3:1)[12,13]. This work will therefore proceed on the basis that $H_2O\cdots$imid is the molecular carrier of the spectrum for which 0^- and 0^+ states are assigned.

Attempts were made to fit transitions of both 0^- and 0^+ states simultaneously, using Pickett's SPFIT/SPCAT suite of programs[47] and a Hamiltonian including one or more Coriolis coupling constants. A range of strategies were tested which included fixing the values of nuclear quadrupole coupling constants when fitting the values of Coriolis coupling constants and repeating the fits after adjusting the range and values of included Coriolis parameters. It was not possible to constrain the fit to a unique solution. It will be shown later that wagging and torsional coordinates each contribute significantly to large amplitude motion in this complex. It is therefore unsurprising that the simple Hamiltonians tested (which were those available within the standard SPFIT/SPCAT package) did not allow the determination of Coriolis coupling terms. The significant variation in centrifugal distortion constants determined for 0^- and 0^+ states of $H_2O\cdots$imid isotopologues is consistent with complex internal dynamics that are not fully represented by the Hamiltonians employed.

Experiments were performed using HDO and $H_2{}^{18}O$ to verify the geometries of the molecular carriers of the assigned spectra and allow the determination of precise bond lengths and angles. Values of spectroscopic parameters for four isotopologues of imid…H_2O (imid$\cdots$

H_2O, imid···DOH, imid···$H_2{}^{18}O$, imid···HOD) and three isotopologues of H_2O···imid (H_2O···imid, $H_2{}^{18}O$···imid, HDO···imid) were determined through fitting of spectroscopic parameters to the measured transition frequencies (Tables S2 and S3). The evaluated rotational constants confirm the expected changes on isotopic substitution. The spectrum of HDO···imid includes spectra of 0^- and 0^+ states which are separated by an interval that is significantly smaller than that observed for the spectrum of the H_2O···imid isotopologue (Figure 3). This is consistent with the proposal that large amplitude motions of the water molecule lead to the observed splittings. Observation of the spectrum of only one isotopologue of HDO···imid suggests that isotopic substitution at either proton of the water sub-unit causes an equal change in the experimentally-determined moments of inertia of this isomer. This is consistent with the proposal that these protons are rapidly interchanged by large amplitude motions. The spectrum of $H_2{}^{18}O$···imid was observed with only weak intensity so transitions of only one state of this isotopologue were fitted. Table S4 allows a comparison of dipole moments, relative energies and percentage differences between experimentally-determined and calculated rotational constants for each of the functionals employed during this work. The final cycles of the fits of spectroscopic parameters are also provided as supplementary data.

Molecular Geometry. Calculated inertial defects and second (planar) moments[48,49] (shown in Table 2) provide insight into the extent of planarity in each complex and are determined free from detailed assumptions about molecular geometry. The inertial defect is calculated as;

$$\Delta_0 = I_c^0 - I_b^0 - I_a^0 \qquad (1)$$

where the moments of inertia, I_a^0, I_b^0, I_c^0 are those appropriate to the *a*, *b* and *c* inertial axes as indicated by the subscripts. Planar moments are defined as

$$P_{\alpha\alpha} = \frac{1}{2}(-I_{\alpha\alpha} + I_{\beta\beta} + I_{\gamma\gamma}) \quad (2)$$

where α, β and γ are permuted cyclically over the a, b, and c inertial axes. It follows from equations 1 and 2 that $P_{cc} = -\frac{1}{2}\Delta_0$. The inertial defect, Δ_0, will be equal to zero where a molecule is planar in the equilibrium geometry[49]. Vibrational effects lead to slight deviations where the moments of inertia employed are those for the zero-point vibrational state. In general, in-plane vibrations contribute positively to Δ_0 while out-of-plane vibrations make negative contributions. The value of Δ_0 is very close to zero for the parent isotopologue of imid···H_2O implying that this isomer is planar in its zero-point vibrational state. The values of Δ_0 and P_c vary significantly for the two sub-states, 0^- and 0^+, of H_2O···imid. The value of $\Delta_0 = -1.8282$ u Å^2 (for the 0^- state) is close to the result expected where the only out-of-plane atoms are two, rigidly-oriented, hydroxylic protons. A value of $\Delta_0 = -1.2783$ u Å^2 is obtained for the 0^+ state implying the same expectation but with the protons of the water sub-unit located closer to the plane defined by the heavy atoms. In any case, the existence of two states suggests that the orientation of the hydroxylic protons is not rigid on the timescale of the molecular rotation. This aspect of the molecular geometry will be explored further below.

Given that rotational constants are available for different isotopologues of each of imid···H_2O and H_2O···imid, it is possible to determine substitution (r_s) coordinates for H and O atoms in the water subunit. These are determined free from detailed assumptions about the geometry of each complex. The results are summarized alongside Costain errors[50] and compared to calculated equilibrium (r_e) coordinates in Table 3. All are calculated using the Kraitchman method[51] as implemented in the program KRA retrieved from the PROSPE website[52]. The method determines only the magnitudes of coordinates so the signs are those

implied by DFT results calculated at the ωB97X-D/aug-cc-pVQZ level. Small r_s coordinates have the largest fractional uncertainties because vibrational contributions to such coordinates are non-negligible. The *c*-axis coordinate of the oxygen atom of imid···H_2O is calculated to be imaginary implying that the oxygen atom lies in the *ab*-plane of the molecule. The *c*-coordinate for the hydrogen that participates in the intermolecular bond is calculated to be only $|c|$ = 0.104(17) Å. Both results are in reasonable agreement with DFT calculations of r_e coordinates even though hydrogen atoms are generally not located to high precision by the r_s method. The DFT results imply that the "free" hydrogen of the water of imid···H_2O, which does not participate in the intermolecular bond, lies 0.6829 Å above the *ab* plane. The *c*-coordinate calculated for this atom by the r_s method is 0.4521(38) Å. These results can be rationalised with the planar geometry implied by the small value of Δ_0 for the parent isotopologue by invoking rapid oscillation of water in the zero-point state of the complex. This oscillation must interchange the geometries where the non-bonding hydrogen is either above or below the plane of the imidazole ring. A similar vibrational motion was inferred by Gou *et al.*[14] for 2-fluoropyridine···H_2O. The value of Δ_0 rises to –0.381(32) u Å^2 for the imid···H_bOD_{nb} isotopologue (Table S2) (where the "b" subscript denotes the proton engaged in the intermolecular hydrogen bond and "nb" denotes the other proton of H_2O). This result places the deuterium atom of the imid···H_bOD_{nb} isotopologue outside the plane of the imidazole ring both in the equilibrium geometry and in the zero-point state. The implied significant change in vibrational motion on substituting H_{nb} for a deuterium atom rationalises significant differences[53] between the DFT-calculated and r_s coordinates of H_{nb}. The latter are calculated while neglecting differences in vibrational energy. The atomic coordinates of imid···H_2O (Table 3) are otherwise highly consistent with the DFT-calculated results.

As noted earlier, two distinct states are observed in the spectrum of H_2O···imid indicating that large amplitude motions occur rapidly on the timescale of the molecular rotation

of this complex. The assumption of rigid rotor behaviour will therefore be unreliable here. However, some insight can be gained through calculation of the r_s coordinates of the oxygen atom. The rotational constants of the 0^- state of $H_2O\cdots$imid and HDO$\cdots$imid are used for this calculation. Under the initial assumption that the geometry of $H_2O\cdots$imid is as shown in Figure 1, the oxygen atom acts as proton acceptor in the intermolecular bond and its location will be somewhat constrained. Rotational constants were determined for only one state of the spectrum of $H_2{}^{18}O\cdots$imid. The assumption that this should be assigned as the 0^- state leads to the best agreement between r_s, r_e and r_0 coordinates. It is also consistent with the expectation that transitions of the 0^- state of $H_2{}^{18}O\cdots$imid will be more intense than those of the 0^+ state by a factor of three. The *c*-coordinate is found to be imaginary while the small magnitude of the determined *b*-coordinate suggests that the atom is indeed located close to the *a*-inertial axis. Alongside the results of the DFT calculations, this analysis confirms the basic geometry of $H_2O\cdots$imid shown in Figure 1 and justifies the earlier assumption that the oxygen atom is relatively constrained by its participation in the intermolecular hydrogen bond.

Reasonable assumptions about the geometry of each complex now allow the determination of r_0 coordinates. In the discussion that follows, the numbering of heavy atoms within imidazole follows the standard convention for *N*-heteroaromatics. Hydrogen atoms of imidazole are numbered according to the carbon or nitrogen to which they are attached (see Figure 1). The determined inertial defects and r_s coordinates establish the connectivities of imid$\cdots H_2O$ and $H_2O\cdots$imid and the planarity of imid$\cdots H_2O$. It is thereby possible to determine r_0 parameters using the STRFIT program[54] available on the PROSPE website[52]. Least squares fitting of structural parameters to the measured moments of inertia for imid$\cdots H_2O$ yields values for the length of the intermolecular hydrogen bond, $r(H_b\cdots N3)$, and the angles that describe the position and in-plane orientation of the water molecule, $\angle(H_b\cdots N3{-}C2)$ and $\angle(O{-}H_b\cdots N3)$, as shown in Table 4. The fit assumes values of dihedral angles that ensure a planar geometry for

imid···H_2O. It assumes that the geometries of the isolated imidazole and water sub-units are equal to the r_0 geometries of the separated monomers. Next, it is necessary to assume values of the ∠(H_{nb}–O–H_b···N3) and ∠(O–H_b···N3–C2) dihedral angles. Each of these parameters may equal either 0 or 180° while still preserving the requirement that the complex is planar.

Fits performed while assuming that ∠(H_{nb}–O–H_b···N3) = 0° do not converge whereas the assumption that ∠(H_{nb}–O–H_b···N3) = 180° allows the fitting of two alternative, model geometries that are each determined with high precision. The results presented in Tables 3 and 4 were determined while assuming ∠(O–H_b···N3–C2) = 0°. An alternative model geometry can be obtained by assuming that this parameter is equal to 180°. Previous studies of isoxazole···H_2O and pyrimidine···H_2O also identified two model geometries that each fitted the experimentally-determined rotational constants. The experimentally-determined values of nuclear quadrupole coupling constants, χ_{aa}(N), were used to identify the correct geometry of isoxazole···H_2O. In the present work, the coordinates of each nitrogen atom are effectively the same in each model geometry, being equal to within 1% of the magnitudes of the coordinates, with the standard deviations associated with the measured values of χ_{aa}(N1) and χ_{aa}(N3) being of comparable magnitude. Fortunately, the DFT calculations of the present work provide another means of identifying the correct geometry. The DFT calculation of the model geometry finds that ∠(O–H_b···N3–C2) = 0°. The assumption that this parameter is equal to the DFT-calculated result then leads to the best agreement between experiment and theory for all other parameters. The r_0 coordinates given in Table 3, and the structural parameters given in Table 4, are selected for this reason. Values of fitted parameters obtained under the alternative assumption that ∠(O–H_b···N3–C2) = 180° are r(H_b···N3) = 2.006(41) Å, ∠(H_b···N3–C2) = 89.7(42)° and ∠(O–H_b···N3) = 146.9(29)°. This set of parameter values would place the H_b and H2 atoms only 2.24 Å apart which would be very close proximity given that the the sum of van

der Waals radii for two hydrogen atoms is 2.4 Å. A list of atomic coordinates for both the preferred, experimentally-determined geometry of imid···H_2O and the other result is given in Table S6.

Consistent with previous studies[8–11] of pyridine···H_2O, pyrazine···H_2O, pyrimidine···H_2O and pyridazine···H_2O, there is a non-linear hydrogen bond in imid···H_2O as a result of a weak, secondary interaction between the oxygen atom of water and the imidazole ring. The angle, ∠(O–H_b···N3), is found to be 171° by DFT calculation and 172.1(26)º by experiment. The values of the r_0 structural parameters shown in Table 4 allow an r(O···H2) distance to be derived as 3.13(8) Å. This is significantly lower than the DFT-calculated result which is determined to be 3.54 Å. The difference is too great to be explained by the fact that hydrogen atoms are not located accurately by the r_s method. The DFT calculation is for the equilibrium geometry whereas the r_0 results employ zero-point rotational constants leading to further inaccuracies. The significant difference between experiment and theory implies that the DFT calculations at the ωB97X-D/aug-cc-pVQZ level model the primary hydrogen bonding interaction in imid···H_2O with reasonable precision but significantly underestimate a weak, secondary interaction within the complex.

The experimental evidence suggests that large amplitude motion occurs in H_2O···imid and that this principally affects the positions of the hydrogen atoms of the water sub-unit. The in-plane angle that defines the position of the oxygen atom relative to the imidazole ring, ∠(O···H1–N1) is fixed equal to the result of the DFT calculation of 174.7º. Noting that the calculated inertial defects suggest that only the hydroxylic protons lie outside the plane, ∠(O···H1–N1–C2) is fixed to 180º such that the oxygen atom is located in the plane of the imidazole sub-unit. A dummy atom, X, positioned between the two hydrogen atoms, on the local C_{2v} axis and in the plane of the H_2O sub-unit, is assumed to lie in the plane of the

imidazole ring such that ∠(X···O···H1–N1) = 0º. This assumption is guided by the results of the DFT calculation and locates the hydrogen atoms symmetrically on either side of the plane of the imidazole ring. The results obtained by fitting other structural parameters under the described constraints are r(O···H1)=2.000(4) Å and ∠(X···O···H1)=159(7)°. These parameter values and the associated atomic coordinates are highly consistent with the DFT results and so included in Tables 3 and 4. It is not possible to determine additional parameters under the reported assumptions. An alternative assumption that ∠(X···O···H1–N1)=180° would imply r(O···H1)=2.001(4) Å and ∠(X···O···H1)=151(7)°. It will be shown that both fitted solutions are within the range of large amplitude motions implied by torsion and wagging of the water molecule. Assuming that ∠(X···O···H1–N1) is equal to either 90° or 270° (which would correspond with transition states identified during PES scans) leads to very similar values for both r(O···H1) and ∠(X···O···H1) but much greater uncertainties. The residuals that describe differences between measured values of rotational constants and those implied by the fitted structures are higher for A_0 than for B_0 and C_0 rotational constants. Evidently, contamination of the rotational constants by large amplitude motions is greater for A_0 than for B_0 and C_0 constants. This is consistent with the inference that large amplitude motions occur primarily in the torsional coordinate defined by ∠(X–O···H1–N1) and the wagging motion defined by ∠(X···O···H1). Earlier studies[12,13] of H_2O···pyrrole and H_2O···indole identified similar large amplitude motions in other *N*-heteroaromatics containing a pyrrolic nitrogen atom.

Potential Energy Scans of Intermolecular Coordinates of H_2O···imid. DFT calculations were performed to generate potential energy surfaces that characterise the large amplitude motions within the H_2O···imid complex. The dummy atom defined earlier, X, was used in the definition of each scanned intermolecular coordinate. Figure 4 presents the potential energy calculated as a function of ∠(X···O···H1) between 130˚ and 210˚. This coordinate represents the

wagging of H_2O with respect to the imidazole ring. The PES is comparatively flat with a shallow minimum at 154˚ separated from another at 200˚ by a barrier of less than 10 cm^{-1}. Figure 5 presents the potential energy as a function of the torsional motion described by the angle formed by the X…O vector and the imidazole plane between 0 and 180˚. The barrier to interconversion between the two minima is 143 cm^{-1}. The energy difference between the minima is less than 10 cm^{-1}. During each of the described 1D PES scans, all other internal coordinates were held fixed at their values calculated at the ωB97X-D/aug-cc-pVQZ level. Evidently, either or both of wagging and internal rotation may contribute to the identified large amplitude motion in H_2O···imid.

Stretching Force Constants and Dissociation Energy. A model described by Millen[55] allows evaluation of the force constant, k_s, of the intermolecular bond for each of imid···H_2O and H_2O···imid. This approach improves on the simplest pseudo-diatomic model by taking some account of the internal geometry of the participating sub-units. It requires that the *a* inertial axis is aligned, or close to aligned with the axis of the intermolecular stretching motion which is true for imid···H_2O and H_2O···imid. It is assumed that stretching modes of Σ symmetry other than the intermolecular mode do not significantly affect the measured centrifugal distortion constant, D_J, and that the geometries of the isolated sub-units do not change significantly on formation of the complex. It is strictly appropriate only for equilibrium values of rotational and centrifugal distortion constants but zero-point quantities are often used given that equilibrium values are rarely available. Under this model, the force constant k_s is expressed as

$$k_s = 16\pi^4(\mu R_{\mathrm{CM}})^2\left[4B_0^4 + 4C_0^4 - \left(B_0^4 - C_0^4\right)^2\left(B_0^4 + C_0^4\right)^2\right]/(hD_J)$$

where μ is the reduced mass, $\mu = \frac{M_{\mathrm{I}}M_{\mathrm{w}}}{M_{\mathrm{I}} + M_{\mathrm{w}}}$, of the pseudodiatomic where M_{I} and M_{w} are the masses of the water and imidazole sub-units respectively, and R_{CM} is the distance between the

centres of mass of these two sub-units. The stretching frequency, ν, is evaluated as $\nu = \frac{1}{2\pi c}\sqrt{\frac{k_s}{\mu}}$ where c is the speed of light. Results for imid···H_2O and H_2O···imid, calculated from the rotational and centrifugal distortion constants of the parent isotopologue, are in Table 5 alongside those for various other complexes where an *N*-heteroaromatic molecule is bound to water. The results shown for pyridine···H_2O are calculated from constants provided in the original work by McKenzie *et al* [9]. For each of pyridine···H_2O and H_2O···imid, two results are given for k_s and ν because two states were observed leading to the determination of two sets of rotational and centrifugal distortion constants. It is apparent that the force constants and vibrational frequencies are higher, on average, where water is acting as the proton acceptor and the *N*-heteroaromatic is the proton donor. The force constant describing the intermolecular bond in imid···H_2O is twice the magnitude of those in each state of pyridine···H_2O. It is not possible to perform an equivalent comparison for H_2O···imid and H_2O···pyrrole because the values of k_s determined for the two states of H_2O···imid are significantly different from each other and from the result for H_2O···pyrrole. It is likely that effects of the described large amplitude motions are convoluted into the centrifugal distortion constants of H_2O···imid and H_2O···pyrrole. The assumption that stretching modes of Σ symmetry other than the intermolecular mode do not significantly affect the measured centrifugal distortion constant will be unreliable for some complexes included in Table 5 where secondary intermolecular interactions additional to the primary hydrogen bond have been described. For these reasons, the broad trends will not be explored further.

5. DISCUSSION

An important conclusion of the present work is that it is possible to generate both imid···H_2O and H_2O···imid within an argon buffer gas undergoing supersonic expansion such

that both complexes can be spectroscopically characterised. This result is notable when viewed alongside previous studies[17]. Zischang *et al.* employed a heated reservoir to introduce imidazole into a helium backing gas and thereby recorded the infrared spectrum of imid···H_2O. The authors reported that their sample preparation conditions had not yielded the H_2O···imid isomer and postulated that this complex might efficiently relax to the imid···H_2O isomer under their experimental conditions. Ruoff *et al.*[56] had earlier explored the competition between kinetic and thermodynamic control within expanding gas samples. They reported that relaxation to lower energy conformers proceeds rapidly within a gas sample that contains a high concentration of argon or krypton but *less* efficiently within a sample of helium or neon. The present experiments allowed the isolation and spectroscopic characterisation of both imid···H_2O and H_2O···imid following co-expansion of a low concentration of imidazole and water in argon. Viewed alongside the work of Ruoff *et al.*[56], the implication of the present experiments is that both imid···H_2O and H_2O···imid might be observable through experiments that employ either helium or neon buffer gas. The experiments of Bhattacherjee *et al*.[18,19] imply a similar conclusion. Zischang *et al.*[17] asked "*where does the first water molecule go in imidazole?*" in the title of their publication and concluded that imid···H_2O is the lower energy of the two isomers of imidazole monohydrate. During the present work, the spectrum of imid···H_2O was observed with higher intensity than that of H_2O···imid. The latter is calculated to have a higher dipole moment than the former ($|\mu_a|$=6.4 D against $|\mu_a|$=5.3 D with other dipole moment components being of similar magnitude) but its spectrum is split into 0^- and 0^+ states by the large amplitude motions illustrated in Figures 4 and 5. Observed transition intensities do not directly correlate with the relative energies of the isomers. Therefore, while the DFT calculations of the present work identify imid···H_2O as the lowest energy configuration of imidazole monohydrate (Table 1), the experimental results presented herein do not themselves present an answer to the question posed by Zischang *et al.*

Table 6 compares geometrical parameters determined for complexes where *N*-heteroaromatics are coordinated by water molecules. Water coordinates to each of pyrazine[8], pyridine[9], pyrimidine[10], pyridazine[11], 1,3,5-triazine[57], 2-fluoropyridine[14], imidazole and isoxazole[15] via a primary hydrogen bond to a pyridinic nitrogen and a secondary interaction between water and the imidazole ring. Competition between these primary and secondary interactions determines the ∠(O–H_b···N3) angle which is greatest (~165º) for those 6-membered rings that are asymmetric while being smaller (~154º) for the more symmetric molecules, pyridine and pyrazine. In general, the primary hydrogen bond, r(H_b···N3), to 5-membered rings is slightly longer than that to 6-membered rings. Unsurprisingly, there are similarities between the results for imid···H_2O and pyridine···H_2O. The length of the primary hydrogen bonding interaction computed[9] for pyridine···H_2O was 1.931 Å whereas the experimental result for r(H_b···N3) of imid···H_2O is 2.024(23) Å. The length of the secondary interaction within imid···H_2O, defined between the oxygen of H_2O and H2 on the imidazole ring, r(O···H2), is determined to be 2.79(6) Å in the r_0 geometry. This result is 0.1 Å longer than the value of 2.69 Å computed for the secondary interaction in pyridine···H_2O. Fewer results are available for a comparison of geometrical parameters where the *N*-heteroaromatic molecule is the proton donor and H_2O is the proton acceptor. The DFT result for the ∠(O···H1–N1) angle of H_2O···imid is 174.7º suggesting that a very weak, secondary interaction between the water sub-unit and the imidazole ring also contributes to the geometry of this isomer. The ∠(X···O···H1) angle ranges from 143º for H_2O···pyrrole to 165º for H_2O···indole. Large amplitude motions affect the observed spectra for all those complexes featured in Table 6 where the *N*-heteroaromatic molecule is the proton donor.

6. CONCLUSIONS

Broadband rotational spectra of two isomers of a complex formed between imidazole and water, imid···H_2O and H_2O···imid, were recorded in the 7.0-18.5 GHz region. Rotational constants, centrifugal distortion constants and nuclear quadrupole coupling constants were determined for both species. In the former, a non-linear hydrogen bond is observed indicating that a secondary interaction is significant in determining the molecular geometry. In the latter, a linear hydrogen bond exists between the oxygen atom of water and the hydrogen attached to the pyrrolic nitrogen of imidazole. Large amplitude motions lead to the observation of two states, 0^- and 0^+, in the spectra of H_2O···imid. The observation that both imid···H_2O and H_2O···imid are kinetically-stable within argon gas undergoing supersonic expansion implies that they have similar energy.

Conflicts of Interest

The authors declare no conflict of interest and these results present no challenge for previous findings.

Supporting Information

PGOPHER output files displaying the results of spectroscopic fits, DFT-calculated geometrical parameters and nuclear quadrupole coupling constants are provided in Supplementary Tables S1-S6.

Acknowledgements

The authors gratefully acknowledge Newcastle University for a research studentship (for E. G.) and the European Research Council for project funding (Grant No. CPFTMW-307000).

This research made use of the Rocket high performance computing service at Newcastle University.

Table 1. Spectroscopic parameters calculated for imid···H_2O and H_2O···imid at the ωB97X-D/aug-cc-pVQZ level of DFT.

	imid···H_2O	H_2O···imid
A_e (MHz)[a]	9608	9570.97
B_e (MHz)[a]	1778.24	1695.37
C_e (MHz)[a]	1507.59	1449.96
$\|\mu_a\|$, $\|\mu_b\|$, $\|\mu_c\|$ (D)	|5.3|, |1.1|, |1.2|	|6.2|, |0.6|, |0|
ΔE (cm^{-1}, kJ mol^{-1})	0, 0	606, 7.25

[a]. The computed A_e, B_e and C_e are the rotational constants at equilibrium whereas the experiment determines A_0, B_0 and C_0 rotational constants of the vibrational ground state.

Table 2. Experimentally-determined spectroscopic parameters fitted to Watson's *S*-reduced Hamiltonian for each of imid···H_2O and H_2O···imid.

	imid···H_2O	H_2O···imid	
		0^-	0^+
A_0 (MHz)	9502.79(43)[a]	9436.97(54)	9520.99(26)
B_0 (MHz)	1826.3929(13)	1663.0101(11)	1662.91298(73)
C_0 (MHz)	1531.9303(10)	1421.1251(13)	1420.74502(72)
D_J (kHz)	1.269(20)	0.487(18)	0.2349(96)
D_{JK} (kHz)	63.03(21)	49.77(25)	59.20(15)
χ_{aa}(N1) (MHz)	1.143(19)	0.923(75)	0.916(45)
$[\chi_{bb}(\mathrm{N1}) - \chi_{cc}(\mathrm{N1})]$ (MHz)	3.712(56)	3.80(46)	4.07(23)
χ_{aa}(N3) (MHz)	–2.889(21)	–1.932(71)	–1.859(44)
$[\chi_{bb}(\mathrm{N3}) - \chi_{cc}(\mathrm{N3})]$ (MHz)	–1.07(11)	–2.66(44)	–2.47(25)
κ [b]	–0.926115(4)	–0.939648(4)	–0.9402073(31)
P_{aa} (u Å^2)	276.7053(12)	302.9729(15)	303.2656(13)
P_{bb} (u Å^2)	53.1839(12)	52.6377(15)	52.4401(13)
P_{cc} (u Å^2)	–0.0029(12)	0.9141(15)	0.6391(13)
Δ (u Å^2)	0.0059(24)	–1.8282(31)	–1.2783(15)
N [c]	60	37	24
σ_{RMS} [d] (kHz)	13.7	13.6	5.8

[a.] Numbers in parentheses are one standard deviation in units of the last significant figure.

[b.] Ray's asymmetry parameter is calculated as $\kappa = \frac{2B_0 - A_0 - C_0}{A_0 - C_0}$

[c.] N and σ_{RMS} are respectively the number of measured transitions and the standard deviation of the fit.

Table 3. Experimentally-determined (r_0, r_s) and DFT-calculated (r_e) atomic coordinates for imid···H_2O and H_2O···imid.

		imid···H_2O		
		a / Å	*b* / Å	*c* / Å
H_b	r_e (calc.)	2.253901	0.141020	–0.054538
	r_s (exp.)	2.25889(77)[a]	0.3339(53)	–0.104(17)
	r_0 (exp.)	2.217(5)	0.178(26)	0[b]
O	r_e (calc.)	3.203723	–0.048453	–0.124829
	r_s (exp.)	3.13460(50)	–0.115(14)	0[c]
	r_0 (exp.)	3.148(2)	–0.0755(9)	0[b]
H_{nb}	r_e (calc.)	3.584692	0.289172	0.682930
	r_s (exp.)	3.62122(47)	0.5218(33)	0.4521(38)
	r_0 (exp.)[a]	3.631(22)	0.760(14)	0[b]
		H_2O···imid		
	Å	*a*	*b*	*c*
O	r_e (calc.)	–3.15362	0.077918	0.00007
	r_s (exp.)	–3.24141(48)	0.042(38)	0[c]
	r_0 (exp.)	–3.2452(38)	–0.018(8)	0

a. Numbers in parentheses are one standard deviation in units of the last significant figure.
b. The r_0 coordinates are those determined under one of two alternative model geometries which fit the rotational constants with high accuracy (see text for details). The coordinates shown are those obtained when the r_0 parameters are as shown in Table 4.
c. Imaginary result is obtained so r_s coordinate is assumed equal to zero.

Table 4. Experimentally-determined (r_0) and DFT-calculated (r_e) structural parameters of imid···H_2O and H_2O···imid.

Parameter[a]	Method	imid···H_2O	Parameter[a]	Method	H_2O···imid
r(H_b···N3) / Å	r_e (calc.)	1.931	r(H1···O) / Å	r_e (calc.)	1.953
	r_0 (exp.)	1.927(27)[b,c]		r_0 (exp.)	2.000(4)[b]
∠(H_b···N3–C2) / º	r_e (calc.)	116	∠(H1···O···X) / º	r_e (calc.)	153
	r_0 (exp.)	99.9(41)		r_0 (exp.)	159(7)
∠(O–H_b···N3) / º	r_e (calc.)	171			
	r_0 (exp.)	172.1(26)			

a. See text and Figure 1 for parameter definitions.
b. Numbers in parentheses are one standard deviation in units of the last significant figure.
c. The r_0 parameters are those determined under one of two alternative model geometries which fit the rotational constants with high accuracy (see text for details).

Table 5. Stretching force constant k_s, stretching wavenumber, $\nu\,/c$, and dissociation energy, D_0, determined for hydrogen bonded complexes described in references 9-12, 15, 56.

	k_s (kg m s^{-2})	$\nu\,/c$ (cm^{-1})
pyridine···H_2O[a]	4.36(11)/5.95(16)[b]	71.0(9)/82.9(11)
1,3,5-triazine···H_2O	9.05	108.1
imid···H_2O	10.69(17)	112.9(9)
pyrimidine···H_2O	13.8	126
pyridazine···H_2O	13.1	122.8
isoxazole···H_2O	26.9(10)	178.6(33)
H_2O···imid[a]	22.0(8)/45.6(1.9)	162(3)/233(5)
H_2O···pyrrole	28	180

a. The two results shown for each of pyridine···H_2O and H_2O···imid are those determined for the 0^- and 0^+ states respectively. For pyridine···H_2O, values for k_s and ν were deduced from the spectroscopic parameters determined in the original work of R. B. Mackenzie *et al.*[9]
b. Numbers in parentheses are one standard deviation in units of the last significant figure.

Table 6. Lengths and geometries of hydrogen bonds reported for complexes described in references 8-13, 15.

Proton donor = H_2O	$r(H_b\cdots N3)$ / Å	$\angle(O–H_b\cdots N3)$ / º
6-membered rings		
pyrazine···H_2O	1.94(2)	152(4)
pyridine ···H_2O [a]	1.95	156
pyrimidine···H_2O	1.98	164.7
pyridazine ···H_2O	2.04	165.5
5-membered rings		
imid···H_2O [b]	1.927(26)	172.1(26)
isoxazole···H_2O	2.1467	141.12
Proton donor = N-heteroaromatic	r(H1···O) / Å	∠(H1···O···X) / º
H_2O···pyrrole	-	143(5)
H_2O···imid [b]	2.000(4)	159(7)
H_2O···indole	2.007(5)	165(5)

[a.] DFT result (ref 9) calculated at the M06-2X/6-311++G(3df,3pd) level.
[b.] Experimentally-determined r_0 parameters (this work).

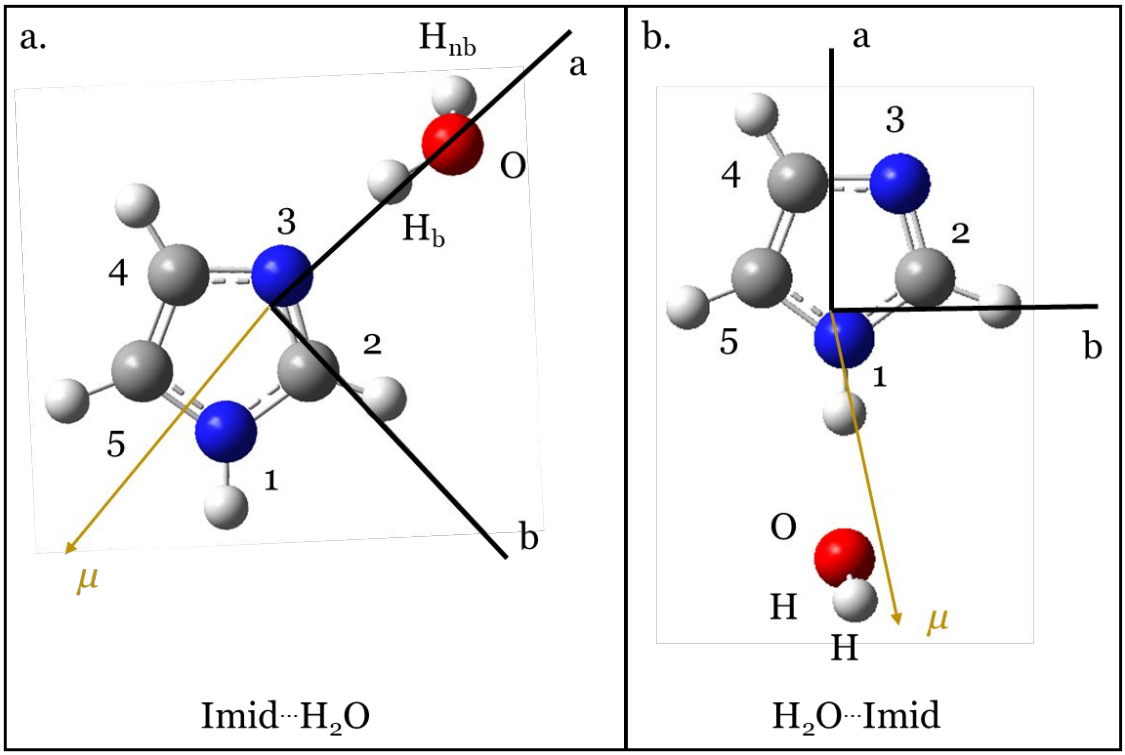

Figure 1. Equilibrium geometries of imid···H_2O and H_2O···imid calculated at the ωB97XD/aug-cc-pVQZ level of theory.

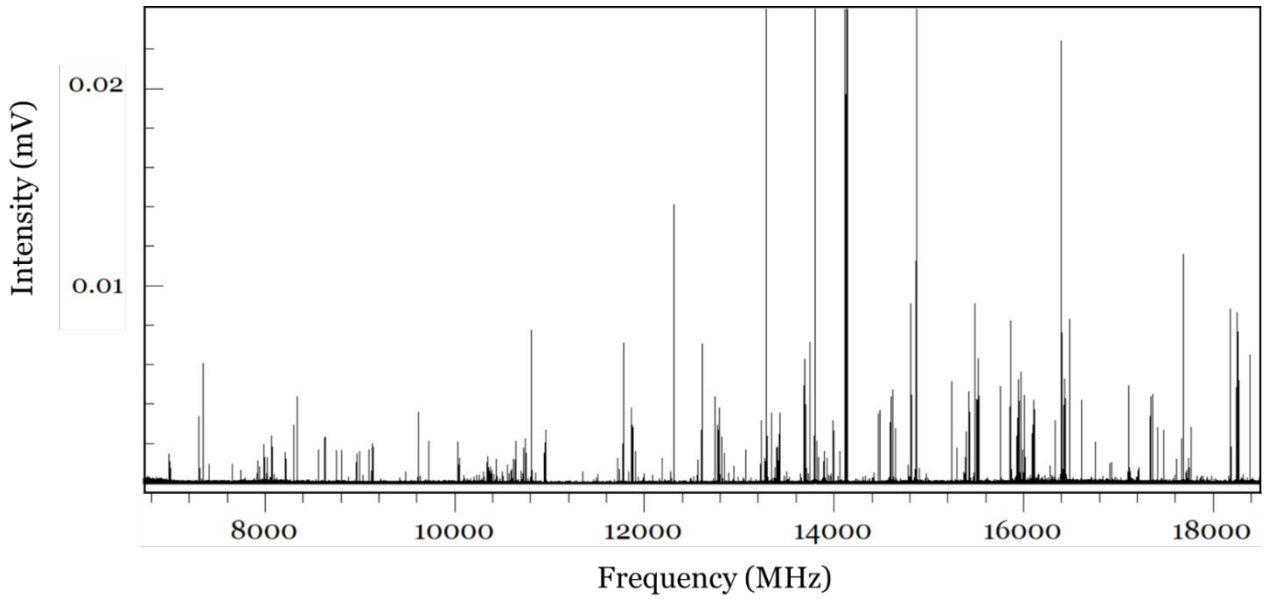

Figure 2. Broadband microwave spectrum between 7.0 and 18.5 GHz recorded over 240k FID's under the experimental conditions described in Section 2.

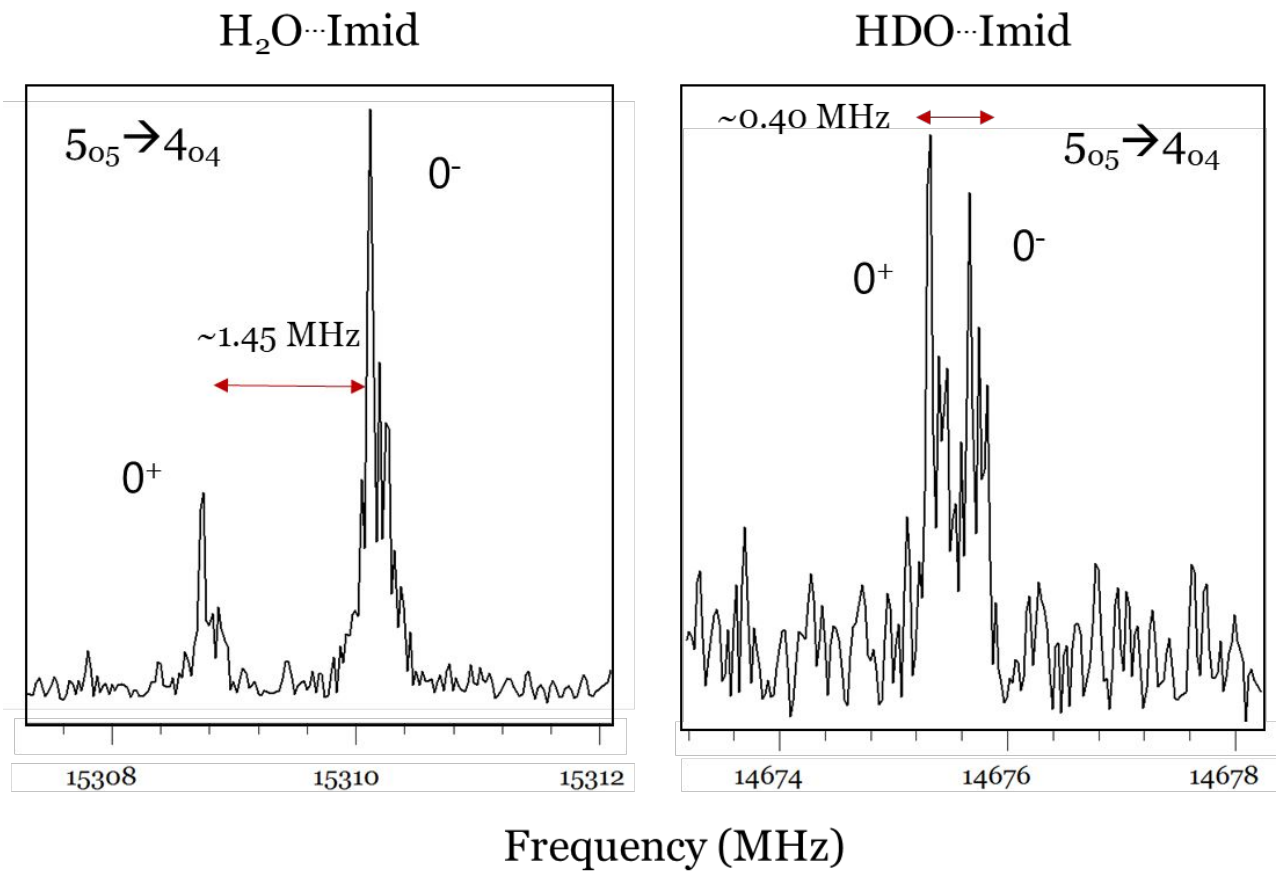

Figure 3. (a, left panel) Expanded section of the $5_{05}\rightarrow4_{04}$ transition of $H_2O\cdots$imid and (b, right panel) the same transition of the HDO···imid isotopologue. Rotational transitions are split into 0^+ and 0^- states. The splitting between the 0^- and 0^+ states decreases upon deuteration implying large amplitude motion of the water molecule.

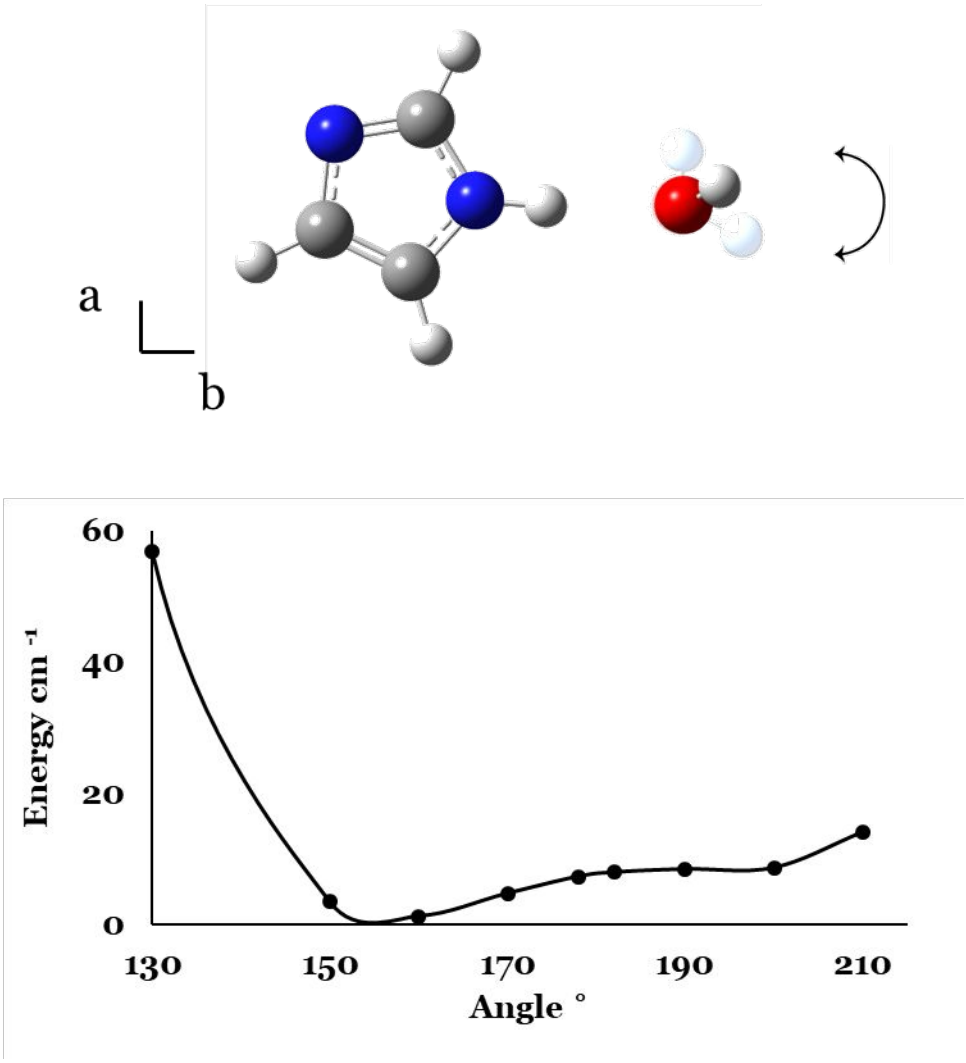

Figure 4. Calculated potential energy surface tracing the wagging motion of $H_2O\cdots$imid at the ωB97X-D/aug-cc-pVQZ level. The transparent white spheres are drawn to illustrate the molecular geometries when $\angle$(X···O···H1) is 90° or 200°, where X is a dummy atom positioned on the local C_{2v} axis of H_2O and between the two hydrogen atoms of water. The trend rises steeply towards higher energy beyond the limits of this plot.

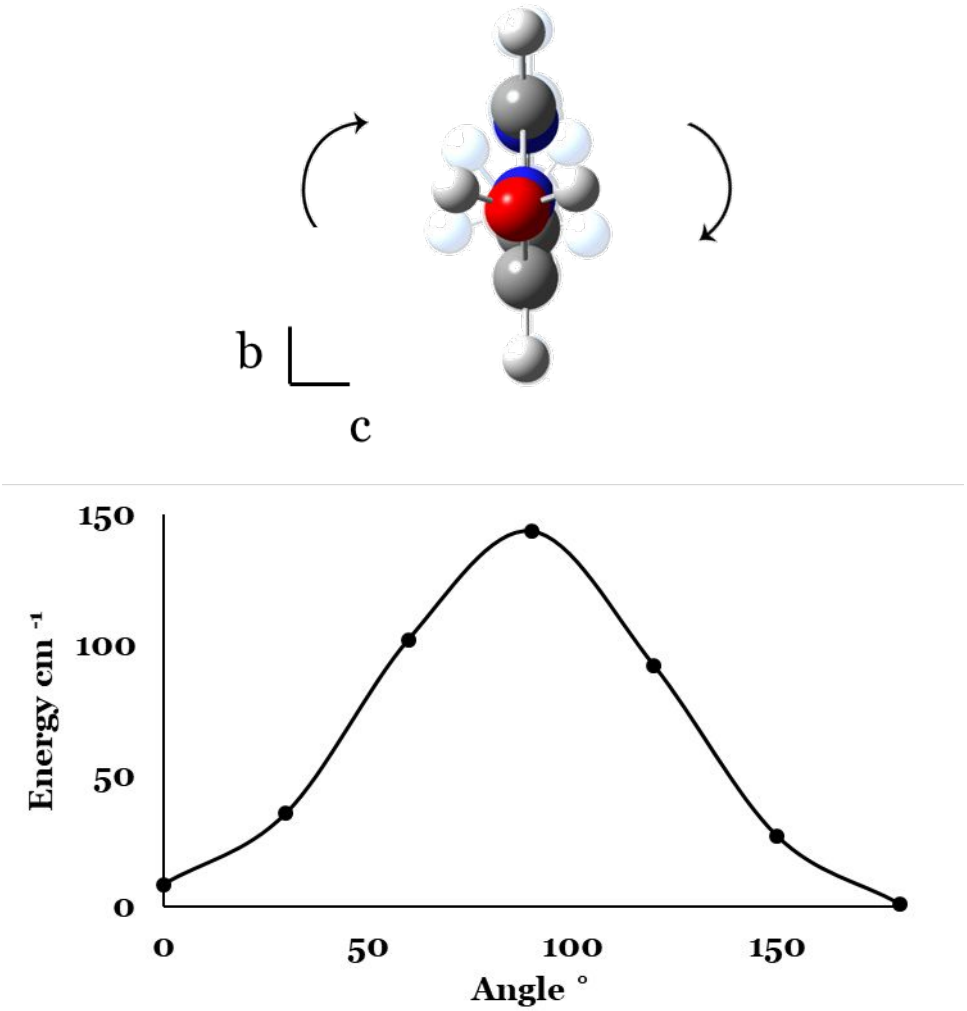

Figure 5. 1D potential energy surface of a torsional motion in $H_2O\cdots$imid defined by the angle formed by the X…O vector and the imidazole plane between 0 and 180˚ at the ωB97X-D/aug-cc-pVQZ level. The white spheres indicate the molecular geometries where this angle is equal to 30° or 120° respectively.

7. REFERENCES

(1) Christen, D.; Griffiths, J. H.; Sheridan, J. The Microwave Spectrum of Imidazole; Complete Structure and the Electron Distribution from Nuclear Quadrupole Coupling Tensors and Dipole Moment Orientation. *Zeitschrift fur Naturforschung - Section A Journal of Physical Sciences*. **1981**, 36 (12), 1378–1385.

(2) Olson, J. S.; Mathews, A. J.; Rohlfs, R. J.; Springer, B. A.; Egeberg, K. D.; Sligar, S. G.; Tame, J.; Renaud, J. P.; Nagai, K. The Role of the Distal Histidine in Myoglobin and Haemoglobin. *Nature* **1988**, 336 (6196), 265–266.

(3) Johnstone, T. C.; Suntharalingam, K.; Lippard, S. J. The Next Generation of Platinum Drugs: Targeted Pt(II) Agents, Nanoparticle Delivery, and Pt(IV) Prodrugs. *Chem. Rev*. **2016**, 116 (5), 3436–3486.

(4) Craven, B. M.; McMullan, R. K.; Bell, J. D.; Freeman, H. C. The Crystal Structure of Imidazole by Neutron Diffraction at 20°C and –150°C. *Acta Crystallogr. Sect. B Struct. Crystallogr. Cryst. Chem*. **1977**, 33 (8), 2585–2589.

(5) Epstein, J.; Ruble, J. R.; Craven, B. M. The Charge Density in Imidazole by X-Ray Diffraction at 103 and 293 K. *Acta Crystallogr. Sect. B Struct. Crystallogr. Cryst. Chem.* **1982**, 38 (1), 140–149.

(6) Caminati, W.; Melandri, S.; Millemaggi, A.; Favero, P. G. Rotational Spectrum of the Imidazole-Argon Complex. *Chem. Phys. Lett*. **1998**, 294 (4–5), 377–380.

(7) Mullaney, J. C.; Zaleski, D. P.; Tew, D. P.; Walker, N. R.; Legon, A. C. Geometry of an Isolated Dimer of Imidazole Characterised by Rotational Spectroscopy and Ab Initio Calculations. *ChemPhysChem* **2016**, 17 (8), 1154–1158.

(8) Caminati, W.; Favero, L. B.; Favero, P. G.; Maris, A.; Melandri, S. Intermolecular Hydrogen Bonding between Water and Pyrazine. *Angew. Chemie Int. Ed*. **1998**, 37 (6), 792–795.

(9) Mackenzie, R. B.; Dewberry, C. T.; Cornelius, R. D.; Smith, C. J.; Leopold, K. R. Multidimensional Large Amplitude Dynamics in the Pyridine-Water Complex. *J. Phys. Chem. A* **2017**, 121 (4), 855–860.

(10) Melandri, S.; Sanz, M. E.; Caminati, W.; Favero, P. G.; Kisiel, Z. The Hydrogen Bond between Water and Aromatic Bases of Biological Interest: An Experimental and Theoretical Study of the 1:1 Complex of Pyrimidine with Water. *J. Am. Chem. Soc*. **1998**, 120 (44), 11504–11509.

(11) Caminati, W.; Moreschini, P.; Favero, P. G. The Hydrogen Bond between Water and Aromatic Bases of Biological Interest: Rotational Spectrum of Pyridazine−Water. *J. Phys. Chem. A* **1998**, 102 (42), 8097–8100.

(12) Tubergen, M. J.; Andrews, A. M.; Kuczkowski, R. L. Microwave Spectrum and Structure of a Hydrogen-Bonded Pyrrole-Water Complex. *J. Phys. Chem*. **1993**, 97 (29), 7451–7457.

(13) Blanco, S.; Lopez, J. C.; Alonso, J. L.; Ottaviani, P.; Camináti, W. Pure Rotational Spectrum and Model Calculations of Indole–Water. *J. Chem. Phys*. **2003**, 119 (2), 880–886.

(14) Gou, Q.; Spada, L.; Vallejo-Lopez, M.; Melandri, S.; Lesarri, A.; Cocinero, E. J.; Caminati, W. Intermolecular Hydrogen Bonding in 2-Fluoropyridine-Water. *ChemistrySelect* **2016**, 1 (6), 1273–1277.

(15) McGlone, S.; Moreschini, P.; Ha, T.-K.; Bauder, A. Microwave Spectra and Structure of an Isoxazole-Water Complex. *Mol. Phys*. **2001**, 99 (16), 1353-1364.

(16) Choi, M. Y.; Miller, R. E. Infrared Laser Spectroscopy of Imidazole Complexes in Helium Nanodroplets: Monomer, Dimer, and Binary Water Complexes. *J. Phys. Chem. A* **2006**, 110 (30), 9344–9351.

(17) Zischang, J.; Lee, J. J.; Suhm, M. A. Communication: Where Does the First Water Molecule Go in Imidazole? *J. Chem. Phys*. **2011**, 135 (6), 61102.

(18) Bhattacherjee, A.; Wategaonkar, S. Conformational Preferences of Monohydrated Clusters of Imidazole Derivatives Revisited. *Phys. Chem. Chem. Phys*. **2015**, 17 (31), 20080–20092.

(19) Bhattacherjee, A.; Wategaonkar, S. Water Bridges Anchored by a C–H···O Hydrogen Bond: The Role of Weak Interactions in Molecular Solvation. *Phys. Chem. Chem. Phys*. **2016**, 18 (40), 27745–27749.

(20) Stephens, S. L.; Mizukami, W.; Tew, D. P.; Walker, N. R.; Legon, A. C. Molecular Geometry of OC...AgI Determined by Broadband Rotational Spectroscopy and Ab Initio Calculations. *J. Chem. Phys*. **2012**, 136 (6), 64306.

(21) Medcraft, C.; Gougoula, E.; Bittner, D. M.; Mullaney, J. C.; Blanco, S.; Tew, D. P.; Walker, N. R.; Legon, A. C. Molecular Geometries and Other Properties of H_2O···AgI and H_3N···AgI as Characterised by Rotational Spectroscopy and Ab Initio Calculations. *J. Chem. Phys*. **2017**, 147 (23), 234308.

(22) Gougoula, E.; Medcraft, C.; Heitkämper, J.; Walker, N. R. Barriers to Internal Rotation in Methylimidazole Isomers Determined by Rotational Spectroscopy. *J. Chem. Phys*. **2019**, 151 (14), 144301.

(23) Frisch, M. J.; Trucks, G. W., Schlegel, H. B.; Robb, M. A.; Cheeseman, J. R.; Scalmani, G; Barone V.; Petersson, H. G. A.; Nakatsuji, H.; Caricato, M.; Li, X.; et al. Gaussian 09, Revision D.01. Gaussian, Inc.: Wallingford CT 2013.

(24) Miehlich, B.; Savin, A.; Stoll, H.; Preuss, H. Results Obtained with the Correlation Energy Density Functionals of Becke and Lee, Yang and Parr. *Chem. Phys. Lett*. **1989**, 157 (3), 200–206.

(25) Becke, A. D. Density-Functional Thermochemistry. III. The Role of Exact Exchange. *J. Chem. Phys*. **1993**, 98 (7), 5648–5652.

(26) Vosko, S. H.; Wilk, L.; Nusair, M. Accurate Spin-Dependent Electron Liquid Correlation Energies for Local Spin Density Calculations: A Critical Analysis. *Can. J. Phys*. **1980**, 58 (8), 1200–1211.

(27) Grimme, S.; Steinmetz, M. Effects of London Dispersion Correction in Density Functional Theory on the Structures of Organic Molecules in the Gas Phase. *Phys. Chem. Chem. Phys*. **2013**, 15 (38), 16031–16042.

(28) Grimme, S.; Ehrlich, S.; Goerigk, L. Effect of the Damping Function in Dispersion Corrected Density Functional Theory. *J. Comput. Chem*. **2011**, 32 (7), 1456–1465.

(29) Dunning, T. H. Gaussian Basis Sets for Use in Correlated Molecular Calculations. I. The Atoms Boron through Neon and Hydrogen. *J. Chem. Phys*. **1989**, 90 (2), 1007–1023.

(30) Kendall, R. A.; Dunning, T. H.; Harrison, R. J. Electron Affinities of the First-Row Atoms Revisited. Systematic Basis Sets and Wave Functions. *J. Chem. Phys*. **1992**, 96 (9), 6796–6806.

(31) Chai, J.-D.; Head-Gordon, M. Long-Range Corrected Hybrid Density Functionals with Damped Atom–Atom Dispersion Corrections. *Phys. Chem. Chem. Phys*. **2008**, 10 (44), 6615–6620.

(32) Goerigk, L.; Grimme, S. A Thorough Benchmark of Density Functional Methods for General Main Group Thermochemistry, Kinetics, and Noncovalent Interactions. *Phys. Chem. Chem. Phys*. **2011**, 13 (14), 6670–6688.

(33) Hoeft, J.; Nair, K. P. R. Millimeter-Wave Rotational Transitions and Molecular Constants of the Diatomic Silver Iodide. *Chem. Phys. Lett*. **1986**, 129 (6), 538–540.

(34) Coudert, L. H.; Lovas, F. J.; Suenram, R. D.; Hougen, J. T. New Measurements of Microwave Transitions in the Water Dimer. *J. Chem. Phys*. **1987**, 87 (11), 6290–6299.

(35) Coudert, L. H.; Hougen, J. T. Analysis of the Microwave and Far Infrared Spectrum of the Water Dimer. *J. Mol. Spectrosc*. **1990**, 139 (2), 259–277.

(36) Snell, R. L.; Schloerb, F. P.; Young, J. S.; Hjalmarson, a.; Friberg, P. Observations of HC_3N, HC_5N, and HC_7N in Molecular Clouds. *Astrophys. J.* **1981**, 244 (1), 45.

(37) Kirby, C.; Kroto, H. W.; Walton, D. R. M. The Microwave Spectrum of Cyanohexatriyne, HC_7N. *J. Mol. Spectrosc*. **1980**, 83 (2), 261–265.

(38) McCarthy, M. C.; Levine, E. S.; Apponi, A. J.; Thaddeus, P. Experimental Structures of the Carbon Chains HC_7N, HC_9N, and $HC_{11}N$ by Isotopic Substitution. *J. Mol. Spectrosc*. **2000**, 203 (1), 75–81.

(39) Boucher, D.; Burie, J.; Demaison, J.; Dubrulle, A.; Legrand, J.; Segard, B. High-Resolution Rotational Spectrum of Methyl Cyanide. *J. Mol. Spectrosc*. **1977**, 64 (2), 290–294.

(40) Simpson, J. B.; Smith, J. G.; Whiffen, D. H. Microwave Spectrum of ICN Including $IC^{15}N$. *J. Mol. Spectrosc*. **1972**, 44 (3), 558–570.

(41) Bjorvatten, T. Molecular Structure and Microwave Spectra of Isotopic Chloro-, Bromo-, and Iodocyanoacetylene. *J. Mol. Struct*. **1974**, 20 (1), 75–82.

(42) Bester, M.; Tanimoto, M.; Vowinkel, B.; Winnewisser, G.; Yamada, K. Rotational Spectrum of Methylcyanoacetylene A New Millimeter Wave Spectrometer. *Zeitschrift fur Naturforschung - Section A Journal of Physical Sciences*. **1983**, 38 (1), 64–67.

(43) Bouchy, A.; Demaison, J.; Roussy, G.; Barriol, J. Microwave Spectrum of Cyanoallene. *J. Mol. Struct*. **1973**, 18 (2), 211–217.

(44) Costain, C. C.; Stoicheff, B. P. Microwave Spectrum, Molecular Structure of Vinyl Cyanide and a Summary of CC, CH Bond Lengths in Simple Molecules. *J. Chem. Phys*. **1959**, 30 (3), 777–782.

(45) Watson, J. K. G. Determination of Centrifugal Distortion Coefficients of Asymmetric-Top Molecules. III. Sextic Coefficients. *J. Chem. Phys*. **1968**, 48 (10), 4517–4524.

(46) Western, C. PGOPHER, a Program for Rotational, Vibrational and Electronic Spectra. *J. Quant. Spectrosc. Radiat. Transf*. **2015**, 186, 221–242.

(47) Pickett, H. M. The Fitting and Prediction of Vibration-Rotation Spectra with Spin Interactions. *J. Mol. Spectrosc*. **1991**, 148 (2), 371–377.

(48) Bohn, R. K.; Montgomery, J. A.; Michels, H. H.; Fournier, J. A. Second Moments and Rotational Spectroscopy. *J. Mol. Spectrosc*. **2016**, 325, 42–49.

(49) Gordy, W.; Cook, R. L. Microwave Molecular Spectra, 3rd.; John Wiley & Sons, Ltd: New York, 1984.

(50) Costain, C. C. Further Comments on the Accuracy of Rs Substitution Structures. *Trans. Am. Crystallogr. Assoc*. **1966**, 2, 157–161.

(51) Kraitchman, J. Determination of Molecular Structure from Microwave Spectroscopic Data. *Am. J. Phys*. **1953**, 21 (1), 17–24.

(52) Kisiel, Z. PROSPE - Programs for ROtational SPEctroscopy http://www.ifpan.edu.pl/~kisiel/prospe.htm. (accessed Jan 5, 2020)

(53) Ubbelohde, A. R.; Gallagher, K. J. Acid-Base Effects in Hydrogen Bonds in Crystals. *Acta Crystallogr*. **1955**, 8 (2), 71–83.

(54) Kisiel, Z. Least-Squares Mass-Dependence Molecular Structures for Selected Weakly Bound Intermolecular Clusters. *J. Mol. Spectrosc*. **2003**, 218 (1), 58–67.

(55) Millen, D. J. Determination of Stretching Force Constants of Weakly Bound Dimers from Centrifugal Distortion Constants. *Can. J. Chem*. **1985**, 63 (7), 1477–1479.

(56) Ruoff, R. S.; Klots, T. D.; Emilsson, T.; Gutowsky, H. S. Relaxation of Conformers and Isomers in Seeded Supersonic Jets of Inert Gases. *J. Chem. Phys*. **1990**, 93 (5), 3142–3150.

(57) Maris, A.; Melandri, S.; Miazzi, M.; Zerbetto, F. Interactions of Aromatic Heterocycles with Water: The Driving Force from Free-Jet Rotational Spectroscopy and Model Electrostatic Calculations. *ChemPhysChem* **2008**, 9 (9), 1303–1308.

Graphical Abstract